







Real-time reactive control of stochastic disturbances in forced turbulent jets

Igor A. Maia  and Peter Jordan 

Pprime Institute, CNRS, Université de Poitiers, ENSMA, 86360 Poitiers, France

André V. G. Cavalieri , Eduardo Martini , and Kenzo Sasaki 

*Divisão de Engenharia Aeronáutica, Instituto Tecnológico de Aeronáutica,
12228-900 São José dos Campos, Brazil*

Flávio J. Silvestre 

Institute of Aeronautics and Astronautics, Technische Universität Berlin, 10623 Berlin, Germany



(Received 2 May 2021; accepted 10 November 2021; published 3 December 2021)

In this work we perform reactive control of stochastic disturbances in forced turbulent jets based on destructive interference. The study is motivated by the success of recent studies in applying this type of control on instability waves in transitional boundary layers and free-shear flows. Linear convective mechanisms in the initial region of turbulent jets are explored in order to perform reactive control, wherein the actuation signal is updated in real time based on sensor measurements performed upstream, resulting in an inverse feedforward approach. The control law is based on empirical transfer functions of the jet response to stochastic forcing and actuation, which are measured experimentally. Since turbulent jets have energy content spread in a number of azimuthal wave numbers, we apply axisymmetric forcing at the nozzle lip in order to be able to perform control using a reduced number of sensors and actuators. The external forcing produces axisymmetric wave packets which possess stochastic phases and amplitudes, akin to turbulent fluctuations found in unforced jets. We demonstrate the successful implementation of real-time reactive control of these disturbances, achieving order-of-magnitude attenuations of associated velocity fluctuations. Control is shown to reduce fluctuation levels over an extensive streamwise range.

DOI: [10.1103/PhysRevFluids.6.123901](https://doi.org/10.1103/PhysRevFluids.6.123901)

I. INTRODUCTION

The turbulent jet issuing from an aircraft engine is one of the main sources of its noise, especially during takeoff. Jet noise is a serious environmental problem which imposes severe restraints on the development of the aviation industry. In addition to its environmental and technological importance, jet noise is also a daunting and compelling scientific problem on account of the difficulty in ascertaining and modeling the flow motions responsible for sound radiation. These represent only a small fraction of the flow energy, making the identification of sound-producing flow structures, and their eventual manipulation, a delicate task. Furthermore, in the Reynolds-number range of interest to the aeronautic industry, the jets often issue from nozzles with turbulent boundary layers. Therefore, the underlying flow motions are inherently unsteady and nonlinear, making the problem even more challenging.

It is now recognized that the peak sound radiation in turbulent jets, which occurs at low angles to the jet axis, is due to wave packets [1,2] generated by convective growth mechanisms similar to those generated by a Kelvin-Helmholtz instability in transitional flows. Wave packets possess a

high degree of spatial organization and characteristic length scales larger than the integral scales of turbulence, which makes them more amenable to modeling. It has indeed been demonstrated in the above mentioned reviews that linear models are capable of describing important aspects of wave packet dynamics in the initial jet region. Understanding and modeling jet dynamics and noise radiation from the point of view of wave packets has also opened up new perspectives for control. Control strategies can be based on the modification of the dynamics of these structures, guided by linear models.

The first attempts to reduce jet noise were based on Lighthill's eighth power law [3]. By simplifying turbulence as a superposition of small incoherent eddies, an order-of-magnitude analysis shows that the acoustic power radiated by turbulence is proportional to U^8 , with U being a reference value for velocity within the flow. In an aircraft engine, noise reduction can thus be achieved, while maintaining the thrust, by increasing its diameter, which in turn decreases the jet exit velocity. Significant reductions in sound pressure levels were obtained between the first generation of turbofan engines and those currently used; however, further increases in engine size are limited by aerodynamic performance and structural issues. Subsequent noise-reduction strategies have explored passive devices consisting of nozzle modifications. Examples of such devices are *tabs* and *chevrons* [4–7] or beveled nozzles [8–10]. Changes in the sound radiation associated with nozzle modifications have often been associated with modifications in the streamwise vorticity field [11]. However, more recently it has been shown [12,13] that flow and acoustic changes produced by chevron nozzles are due to a reduction in wave packet growth rates.

Active control has also been widely applied to jets. There exists a great body of work dedicated to understanding jet response to an external forcing. Early works usually made use of acoustic excitation to force axisymmetric or helical wave packets and study their streamwise evolution. In their seminal work, Crow and Champagne [14] conducted a series of flow visualization and hot-wire experiments aimed at better discerning the wave packet signature in the turbulent field and enhancing their underlying order by harmonic forcing. They showed that the imposed forcing raises the coherent-structure amplitudes above background levels, making their identification in the jet easier. Another important finding of their work was the possibility to obtain a regime of linear response to the forcing: provided that the amplitude was small enough, the amplitude of the forced disturbances grows linearly with forcing amplitude up to a certain streamwise position, in good agreement with existing linear models for unforced jets. These results were confirmed by the subsequent near field measurements of Moore [15], who also showed that the forced wave packets produced a clear and strong signature in the sound field. A number of studies followed that aimed at associating flow and/or acoustic modifications introduced by external forcing with the dynamics of harmonically forced wave packets [16–27].

More recently, fluidic actuation using microjets [28–35] and plasma [36–39] actuators has also been widely diffused. These works have been important insofar as they demonstrate that the jet responds to excitation at a broad range of frequencies and azimuthal wave numbers, and that its associated acoustic field can be modified. Furthermore, linear models can be used to understand the dynamics of jet response, as shown by Sinha *et al.* [39], which opens up clear possibilities to use knowledge of linear growth mechanisms in the initial jet region in order to inform control strategies.

One important concept in flow control regards the difference between open-loop and reactive control schemes. In the first case, the actuation signal is steady and remains independent with respect to changes in the flow state, whereas in the second case information regarding the flow states is used to provide an online update of the actuating signal. The second situation is, of course, more challenging from conceptual and practical points of view. Real-time reactive control is often applied to flows with low or moderate Reynolds numbers, where the aim is to avoid or delay transition to turbulence. This can be accomplished in situations where the laminar solution is linearly stable [40], and/or with mild amplification of incoming disturbances [41]. But, as pointed out above, jets with high Reynolds numbers are usually fully turbulent; moreover, they strongly amplify upstream disturbances through a process associated with convective non-normality [42]. In such cases, it is unlikely that the laminar solution may be recovered by closed-loop control. However, turbulent jets

exhibit wave packets whose underlying dynamics can be modeled, to a large extent, using linear models. In that context, reduced-order models based on the linearized equations of motion appear as candidates to provide suitable control-law designs. This is usually done in transition control, and the wealth of methods developed for that application may then become pertinent to turbulent jet control.

A. Transition control

Over the past decades, flow control has become an interdisciplinary field, in which classic control theory is associated with knowledge of fluid systems, data assimilation, and experimental actuation techniques, yielding a variety of approaches that can be applied to different flow configurations [43,44]. Early applications of control theory to fluid systems include the works of Moin and Bewley [45] and Joshi *et al.* [46], who controlled turbulent channel flows using full-state information, Högberg *et al.* [47], who implemented partial-state information control of a transitional channel flow, and Chevalier *et al.* [48], who controlled spatially growing boundary layers.

However, for flows whose Reynolds numbers are of interest to the aerospace industry, the high number of degrees of freedom of the system to be controlled poses a considerable obstacle to the practical application of control theory. Due to the nonlinearity and high dimension of such fluid systems, the design of control strategies often relies on reduced-order models (ROMs). ROMs may be obtained via linearization of the equations of motion around a suitable point. For laminar flows, linearization around a steady-state solution yields a mathematically rigorous procedure to study the development of flow disturbances around the steady field; for turbulent flows, linearization around the time-averaged flow is often used, following Crighton and Gaster's [49] idea that turbulence "establishes an equivalent laminar flow profile". However, the procedure is not exact, since the Reynolds stresses are neglected in the linearization process, and its validity needs to be verified *a posteriori*. This caveat can be partially addressed in the framework of resolvent analysis [50], wherein the nonlinear Reynolds stresses can be treated as an external forcing that drives the mean-flow-based linear operators.

Many flows of interest exhibit organized structures whose underlying dynamics can be modeled, to a large extent, as instability waves. Linear stability theory (including mean-flow-based linear stability) then appears as a candidate to provide suitable control-law designs. Specifically, when the linearized equations are written in state-space form, stability and control theory can be unified in an *input-output* framework [51]. The models can then be associated with optimal control design tools such as Linear Quadratic Regulator (LQR) and Linear Quadratic Gaussian (LQG). This has been done, for instance, by Akervik *et al.* [52] to control a separated boundary layer flow, by Barbagallo *et al.* [53] for a flow over an open cavity, and by Barbagallo *et al.* [54] to control a flow over a backward-facing step. Extensive reviews of tools and techniques developed for the control of transitional flows in an input-output framework have been provided by Bagheri *et al.* [51], Sipp *et al.* [55], Sipp and Schmid [56], and Schmid and Sipp [57].

For *oscillator* flows, which are globally unstable, suitable ROMs can also be obtained by Galerkin methods, wherein a basis consisting of eigenmodes of a global stability problem describing the (usually low dimensional) unstable subspace is combined with a basis consisting of balanced modes describing the higher-dimensional stable subspace [53,56]. The situation is different for *amplifier* flows, where upstream disturbances (intrinsic or external), usually broadband, are amplified by convective instabilities such as Tollmien-Schlichting waves in boundary layers or Kelvin-Helmholtz instabilities in jets and mixing. Alternatively, amplification can also be attained by nonmodal mechanisms, such as lift-up, the Orr mechanism, or transient growth [58]. In this context, modeling any environmental or external noise that can be amplified by the flow and incorporating it in the control design becomes of fundamental importance. But Galerkin models are not appropriate for modeling the disturbance environment [56,57], which makes them unsuitable for amplifier flows.

Control of amplifier flows is thus a more challenging task, both on account of their broadband energy spectrum and their sensitivity to incoming perturbations and ambient noise. As pointed out by Schmid and Sipp [57], model-based control strategies require models for environmental and measurement noise; but simplifying assumptions about the nature of these can have a negative impact on control performance and robustness, even if the incoming disturbances can be measured accurately. A way to circumvent this issue is using model-free adaptive schemes [59]. The advantage, however, of using a model-based controller such as LQR or LQG is that they can provide physical insight of the problem permitting, for example, sensor-actuator placement and actuation shape optimizations.

Linear models based on convective instability mechanisms in amplifier flows have indeed been explored with a view to providing control laws based on feedforward schemes, with actuators often placed downstream of measurement positions. Linearity then offers the possibility of eliminating disturbances through a simple superposition of waves in a destructive interference pattern. For instance, reactive control based on cancellation of Tollmien-Schlichting waves in flat plate boundary layers has been carried out numerically by Laurien and Kleiser [60], wherein the authors report order-of-magnitude reductions at single frequencies. Li and Gaster [61] build on this approach by accounting for broadband perturbations. Using solutions of a locally parallel linear stability analysis, the authors were able to derive theoretical input/output transfer functions. The feedforward control strategy obtained was able to inhibit the growth of the instability waves over a significant portion of the flow. More recently, this approach has been extended by the use of the parabolized stability equations (PSE), which account for streamwise changes in the mean flow. PSE has been used to provide theoretical transfer functions for estimation in turbulent jets [62] and to perform reactive control on transitional boundary layers [63] and mixing layers [64] in numerical simulations. Apart from the work of Li and Gaster [61], other examples of experimental model-based studies are those of Fabbiane *et al.* [41] and Tol *et al.* [65] to the control of Tollmien-Schlichting waves.

Data-driven techniques such as system identification [66,67] are also suitable for amplifier flows. They rely on the determination of a link between the system inputs and outputs through direct flow observations. An example of such approaches is ARMAX (Auto-Regressive-Moving-Average-exogenous), which has been used by Hervé *et al.* [68] to perform control on a flow over a backward-facing step. System identification techniques have also been used experimentally in the control of turbulent boundary layers [69], laminar-turbulent transition on two-dimensional wings [70], and in channel flow [71].

A wave cancellation approach based on system identification has been compared to optimal linear model-based control by Sasaki *et al.* [63] to the control of Tollmien-Schlichting waves. Their work has shown that optimal linear control theory produces a similar control law and a comparable performance to the simpler, system-identification-based wave cancellation approach, suggesting that the former is underpinned by the latter. Furthermore, it has been shown that the *inverse feedforward* scheme developed in that study can be associated with both model-based and system identification approaches.

B. Application to turbulent jets

Our goal in this work is to perform experimental reactive control of a turbulent jet, which is a classic example of amplifier flow. We cannot, unfortunately, make use of the great variety of existing experimental approaches to the control of oscillators. The review by Cattafesta *et al.* [72] reports many studies which perform control on flows over open cavities, for instance, successfully suppressing single or multiple tones (see [73–76], to cite just a few). Cattafesta *et al.* [72] divide closed-loop control techniques for oscillators roughly into two categories: quasistatic and dynamic. The first constitutes a slow modulation of an open-loop signal in order to obtain a phase locking of instabilities. This strategy is suitable to control the tonal peaks that characterize the spectrum of cavity flows; they are, however, not adapted to amplifiers, in which the phases of the broadband disturbances are frequency dependent and, in the case of the turbulent jet, are distorted as they evolve downstream [77]. Dynamic schemes involve the combination of optimal control theory with

a reduced basis for the flow. However, some of the control algorithms developed in this framework, such as pole placement, are also not meaningful for amplifiers, since in this case the dynamics cannot be related to a few global modes.

Here instead we borrow the inverse feedforward technique developed for transition control [63,64] and which has been recently applied experimentally to suppress Tollmien-Schlichting waves [78]. We reiterate that our goal is to perform reactive control [79,80], wherein the actuation signal is updated in real time based on sensor measurements used to detect the target disturbances. In this sense this work differs from previous open-loop [28–39] and modulated open-loop (extremum-seeking) [81–85] techniques. We emphasize, however, that we focus on jets with fully turbulent boundary layers; our goal is thus to control turbulent disturbances, and should not be thought of as a transition delay mechanism. An important step towards this goal has been made in the works of Kopiev *et al.* [86] and Bychkov *et al.* [87], wherein harmonically forced disturbances have been controlled in turbulent jets through wave cancellation.

However, extending the approach from harmonic to broadband disturbances is not a trivial step, due to the stochastic nature of the underlying unsteady fluctuations involved. The works of Wei and Freund [88] and Kim *et al.* [89] have addressed the problem of controlling such disturbances in numerical simulations of a two-dimensional mixing layer and a turbulent jet, respectively, with a view to obtaining noise reductions. Their approach relies on direct and adjoint solutions of a direct numerical simulation (in the case of the mixing layer) and a large-eddy simulation (in the case of the turbulent jet). Solutions to adjoint equations reveal regions of high sensitivity where external forcing can be used to reduce a particular cost functional. Both studies report significant noise reductions and, perhaps more importantly, shed light on the mechanism of noise reduction by disruption of axisymmetric wave packets (2D wave packets in the mixing layer). While this kind of adjoint-based approach can and should be used to provide guidance, it cannot, for the moment, directly provide a control law for implementation in an experiment. The possibility of performing real-time, reactive control of stochastic disturbances in turbulent jets remains unassessed.

We tackle this problem in an experiment designed to perform real-time reactive control of forced jets. The challenge of controlling high-Reynolds-number jet turbulence experimentally is considerable, and thus we have restricted our analysis to a forced flow, where broadband axisymmetric forcing is artificially introduced at the nozzle lip. The goal of the forcing is to increase wave packet amplitudes, in the spirit of what was done by Crow and Champagne [14] and Moore [15], making them easier to identify and control. Unforced jets have an energy content that is spread across a broad range of azimuthal wave numbers, and would thus require a high number of sensors in order to measure high-order azimuthal modes without spatial aliasing. In this sense, forcing the axisymmetric mode allows us to greatly simplify the sensor configuration, which involves an array of microphones in the irrotational near field and a target hot wire on the jet center line. The experiments are performed at low Mach number due to technical limitations of the current setup. Our primary goal here is not explicitly controlling some objective situated on the sound field, but instead canceling the axisymmetric hydrodynamic wave packets which are known to radiate noise at low polar angles. The convective growth mechanisms targeted by the present control approach also exist at higher Mach and Reynolds numbers, without major changes in their dynamics [1,2]. Therefore, the present strategy is not restricted to low-Mach-number jets; it can be rather thought of as a first step towards applications at higher Mach and Reynolds numbers.

Our control scheme is based on recent developments made in the control of transitional Tollmien-Schlichting waves in transitional mixing layers [64] and boundary layers [63,78]; here we benefit from linear convective growth mechanisms present in the initial jet region, which makes them also amenable to this kind of linear inverse feedforward control. We also build upon a considerable body of previous work aforementioned that demonstrated the possibility of exciting the jet through external forcing and understanding jet response in terms of wave packet dynamics.

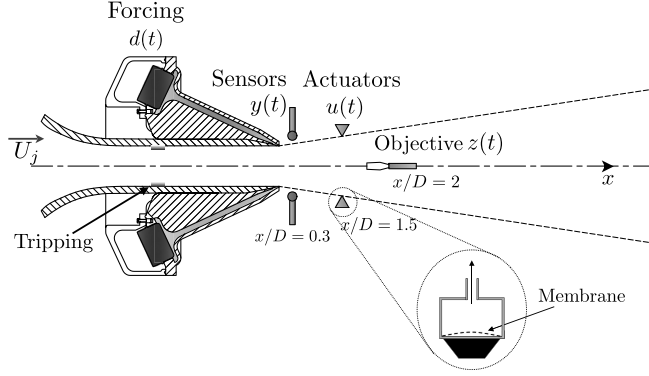


FIG. 1. Schematic of control experiment showing the relative position of inputs and outputs. Forcing (at the nozzle lip) and actuation consist of synthetic jets generated by loudspeakers; the sensors are microphones situated in the near-pressure field of the jet, immediately outside of the shear layer; the objective consists of streamwise velocity measurements performed by a hot wire at the jet centerline. The boundary layer is tripped inside the nozzle by a strip of carborundum particles placed 2.5 diameters upstream of the exit plane, so as to produce a fully turbulent jet.

The rest of the paper is organized as follows. In Sec. II we present the experimental setup, followed by a description of the control law design in Sec. III. The results of the real-time reactive control experiment are presented in Sec. IV and in Sec. V we present the conclusions of the study.

II. EXPERIMENTAL SETUP

The experiments were carried out at the Pprime Institute, in Poitiers, France. The jet Mach ($Ma = U_j/c_\infty$) and Reynolds ($Re = U_j D/\nu$) numbers are 0.05 and 5×10^4 , respectively, with U_j the jet exit velocity, c_∞ the ambient speed of sound, D the jet diameter, and ν the kinematic viscosity of the air. The nozzle diameter is 50 mm.

The control setup consists of four elements: forcing, sensors, actuators, and objective (Fig. 1). The forcing, d , is provided by synthetic jets generated by a system of eight loudspeakers (model AURA NSW 2-236-8AT) equally distributed in the azimuthal direction and mounted on a conical structure fitted on the nozzle. The speakers operate in phase, so as to force axisymmetric disturbances. The synthetic jets exit through a $0.01D$ annular gap and force the main jet at the nozzle lip. Downstream actuators are used to cancel axisymmetric wave packets generated at the nozzle exit by the forcing system. A ring of six 1/4-in. microphones is placed in the near pressure field at a streamwise position of $0.3D$ from the nozzle exit. The axisymmetric pressure mode measured by the microphones gives the input signal, y , for the control law. The actuation, u , also consists of synthetic jets generated by synchronized loudspeakers. Six AURA 1-205-8 A speakers are used to drive synthetic jets on a ring array placed immediately outside of the shear layer at a streamwise position of $1.5D$. The speakers are placed inside cavities whose apertures point towards the center of the main jet. Finally, the objective, z , consists of streamwise velocity measurements performed using a hot wire situated on the jet center line downstream of the actuators, at $x/D = 2$.

Here we choose to conduct the control experiment in the initial jet region, where we can profit from the considerable knowledge of the physics underpinning the growth of disturbances [1,2]. Another possibility would be to perform estimation and control inside the nozzle. It has been recently shown [90] that there is a clear link between wave packets in turbulent jets and coherent structures in the nozzle boundary layer, suggesting that the latter drive the former. The lower disturbance amplitudes and the higher receptivity of the flow would provide clear advantages in performing control in the nozzle. However, further study building on that of Kaplan *et al.* [90]

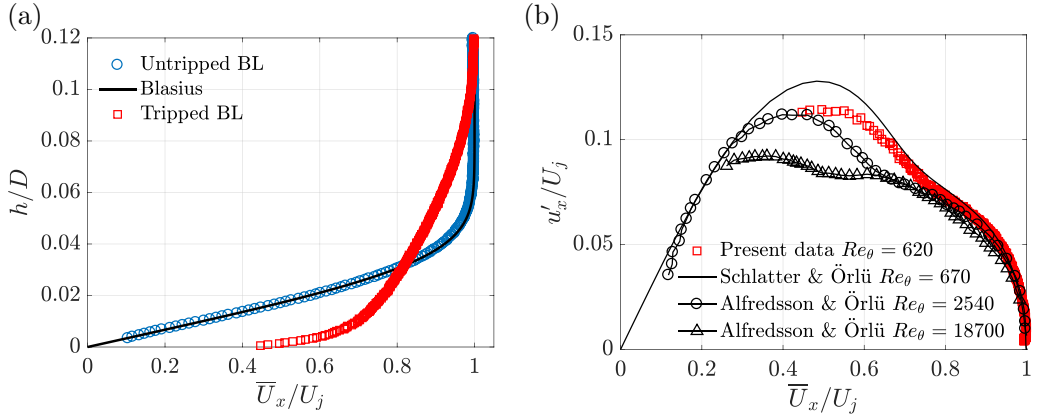


FIG. 2. (a) Mean boundary layer (BL) profiles at the nozzle exit plane. The untripped boundary layer is compared to the Blasius solution for a laminar boundary layer. \bar{U}_x is the mean streamwise velocity and h is the normal distance from the wall. (b) Tripped BL diagnostic plot. The present data is compared to experiments from Örlü and Alfredsson [98] and direct numerical simulation (DNS) data from Schlatter and Örlü [99].

is still needed in order to derive suitable transfer functions between coherent wave packets in the turbulent boundary layer and in the jet.

The nozzle boundary layer is tripped $2.5D$ upstream of the exit plane, to make sure the jet is fully turbulent. Figure 2 shows boundary layer profiles at the nozzle exit plane. The mean boundary layer profile from the untripped nozzle agrees well with the Blasius solution for a laminar boundary layer. The tripped boundary layer is characterized in terms of the *diagnostic plot* proposed by Alfredsson and Örlü [91] to assess near-wall turbulent data independent of friction velocity and wall position and compare with other experimental and numerical data of turbulent boundary layers subject to zero-pressure gradient. The present data follows the trends expected of turbulent boundary layers. The shape of the diagnostic plot and peak rms values u'_x/U_j are in reasonable agreement with data from a similar Re_{δ_2} boundary layer. Also, the peak is shifted towards lower values of \bar{U}_x/U_j with respect to higher Re_{δ_2} flows, as predicted by Alfredsson and Örlü [91]. This shows that the tripping successfully provokes transition to turbulence, leading to a canonical boundary layer upstream of the nozzle exit. Peak turbulence intensity levels on the shear layer just downstream of the exit plane, where control is applied, were found to be between 12% and 15%, which is typical for jets issuing from nozzles with turbulent boundary layers [92–97].

The present sensor/actuator configuration, with reference sensors positioned upstream of the actuators, results in a disturbance feedforward (or inverse feedforward) scheme, which is suitable for convectively unstable (amplifier) flows. Different relative positions of sensors and actuators have been investigated by Belson *et al.* [100]. As shown in that study, the best controller performance for amplifier flows is achieved in the disturbance feedforward configuration. However, the performance of the feedforward controller is severely degraded in *off-design* conditions or in the presence of unmodeled disturbances. For those cases, a feedback configuration, in which sensors detect the effect of actuators placed upstream, is shown to provide a more robust framework. Alternatively, robustness can be achieved by adaptive algorithms in which the downstream objective, z , is used to modify the actuation signal by a modification of the kernel in order to adapt to changing flow conditions. As pointed out by Belson *et al.* [100], in feedback configurations where the sensor is far downstream of the actuators, the large time delays involved may lead to a large number of zeros in the feedback transfer functions, resulting in uncontrollable frequencies. Therefore, a good trade-off between performance and robustness is usually achieved for small separations distances between actuators and sensors. However, in our experimental setup a very small separation distance would lead to an excessive acoustic contamination of the microphone

readings by the actuators, as explained in Sec. III. Therefore, here we focus only on an inverse feedforward approach; but feedback and robust control approaches ought to be pursued in future work.

III. CONTROL LAW DESIGN

The control law design is based on that of Sasaki *et al.* [63,64]. We seek to eliminate z , which corresponds to a linear combination of the estimated velocity fluctuation with the effect of the actuation at an established position. The framework is evaluated in the frequency domain, given in terms of estimation and actuation transfer functions, as

$$Z(\omega) = G_{\tilde{y}z}(\omega)\tilde{Y}(\omega) + G_{uz}(\omega)U(\omega), \quad (1)$$

where capital letters denote frequency-domain quantities and ω is the angular frequency. \tilde{Y} denotes a measurement which is uncontaminated by the actuation signal. During the transfer-function identification step, responses to forcing and actuation are analyzed separately, which allows us to measure \tilde{Y} . However, in the real-time experiment, with simultaneous forcing and actuation, sensor readings are affected by the acoustic signature of the actuators, due to their proximity in the current setup. This is explicitly taken into account in the expression for the actuation signal, Eq. (8), which is later inserted in Eq. (1) to obtain the control kernels, as explained shortly. $G_{\tilde{y}z}$ and G_{uz} are the sensor/objective and actuator/objective transfer functions, respectively. They are defined as the ratio between the cross-spectral densities (CSD) of inputs and outputs ($S_{\tilde{y}z}$ and S_{uz}) and the power-spectral densities (PSDs) of inputs ($S_{\tilde{y}\tilde{y}}$ and S_{uu}),

$$G_{\tilde{y}z} = \frac{S_{\tilde{y}z}}{S_{\tilde{y}\tilde{y}}}, \quad (2)$$

$$G_{uz} = \frac{S_{uz}}{S_{uu}}. \quad (3)$$

CSDs and PSDs have been computed using Welch's method,

$$S_{\tilde{y}z}(\omega) = \frac{1}{N_b} \sum_{k=1}^{N_b} \tilde{Y}(\omega)^{(k)} Z(\omega)^{* (k)}, \quad (4)$$

$$S_{uz}(\omega) = \frac{1}{N_b} \sum_{k=1}^{N_b} U(\omega)^{(k)} Z(\omega)^{* (k)}, \quad (5)$$

$$S_{\tilde{y}\tilde{y}}(\omega) = \frac{1}{N_b} \sum_{k=1}^{N_b} \tilde{Y}(\omega)^{(k)} \tilde{Y}(\omega)^{* (k)}, \quad (6)$$

$$S_{uu}(\omega) = \frac{1}{N_b} \sum_{k=1}^{N_b} U(\omega)^{(k)} U(\omega)^{* (k)}, \quad (7)$$

wherein Fourier transforms \tilde{Y} , U , and Z were computed for different time blocks (following the ergodic hypothesis) with the same length and averaged. In Eqs. (4)–(7), k denotes an individual time block and $*$ denotes complex conjugation. A total of $N_b = 216$ blocks with 50% overlapping have been used. A Hanning window has been applied to each block to reduce spectral leakage. We set an acquisition frequency of 30 kHz and a measurement time of 30 s, which is far superior to the characteristic time scales of the flow, thus assuring the convergence of the single- and two-point statistics necessary for transfer-function computation.

The actuation signal is expressed as a linear combination of the uncontaminated sensor reading and an actuator/sensor transfer function:

$$U(\omega) = K_y(\omega)(\tilde{Y}(\omega) + G_{u\tilde{y}}(\omega)U(\omega)), \quad (8)$$

where $G_{u\tilde{y}}$ is computed through the same procedure described for $G_{\tilde{y}z}$ and G_{uz} . Here $G_{u\tilde{y}}$ is included with the sole purpose of accounting for the contamination of the measurements by the actuators. As shown in Appendix A, this contamination is purely acoustic; the hydrodynamic perturbations introduced by the actuators in order to cancel the incoming perturbations travel downstream and remain undetected by the sensors, due to the strong convective character of the flow. The contamination transfer function thus only removes the acoustic component from the control kernels, preventing them from introducing undesirable noise in the actuation signal. This should not, therefore, be confused with a classic feedback configuration, where the actuation is modified in closed loop by a downstream sensor. K_y is the control kernel, which is obtained by inserting Eq. (8) into Eq. (1) and setting $Z(\omega) = 0$, yielding

$$K_y(\omega) = -\frac{G_{y\tilde{z}}(\omega)}{G_{uz}(\omega) - G_{u\tilde{y}}(\omega)G_{y\tilde{z}}(\omega)}. \quad (9)$$

where the superscript \sim is henceforth dropped for simplicity. This procedure to compute the gain might lead to noise in regions of the spectrum where $G_{y\tilde{z}}$ and G_{uz} have low amplitudes, which might cause the amplification of eventual noise and the appearance of uncontrollable frequencies. In order to avoid this issue, kernels have been filtered in the frequency bands of forcing and actuation, which will be defined shortly. Another strategy to avoid noise amplification is the use of a real-valued penalization term in the actuation [63,101], reducing the kernel amplitudes outside of a desired band. Sasaki *et al.* [63] has outlined a procedure in which the value of the penalization is selected based on analyses of an integral measure of the kernel amplitude and its expected theoretical performance. This is a more rigorous approach to obtain balanced, optimized kernels, and is something to be considered in future experimental applications.

In the time domain, the control law is given by

$$u_y(t) = \int_0^\infty k_y(\tau)y(t - \tau)d\tau, \quad (10)$$

where k_y is the inverse Fourier transform of K_y and y is a sensor reading containing disturbance information plus the feedback contamination. Although $k_y(\tau)$ is not strictly zero for $\tau < 0$ the convolution can only be applied in real time by considering positive τ , as discussed by Sasaki *et al.* [64], so the kernel here is truncated to its causal part. Given the present arrangement of sensors and actuators, the causal part should be expected to contain much of the information relevant for control.

In this configuration, the sensor is placed upstream of the actuator, which is suitable for convection-dominated flows such as the jet. It is worth emphasizing that the system is reactive, as the actuation signal is computed in real time based on a measurement of the state (in this case hydrodynamic pressure fluctuations) through the convolution defined in Eq. (10); in this regard, this is different from “classic” feedforward, where actuation is predetermined, without adapting to unsteady changes in the flow. The present reactive control approach can thus be defined as *inverse feedforward* or *disturbance feedforward* [57].

We also consider a simplified control problem in which we eliminate the intermediary step of measuring the disturbances upstream of the objective position. This is done by expressing the output as a linear combination of the introduced disturbances and actuation only, leading to the simplified control kernel,

$$K_d(\omega) = -\frac{G_{dz}(\omega)}{G_{uz}(\omega)}, \quad (11)$$

$$u_d(t) = \int_0^\infty k_d(\tau)d(t - \tau)d\tau, \quad (12)$$

with k_d the inverse Fourier transform of K_d . The disturbance, d , acts then at the same time as an external disturbance and an input for the controller. This can be considered as a preliminary trial approach for control. It allows us to ascertain whether destructive interference is possible in a

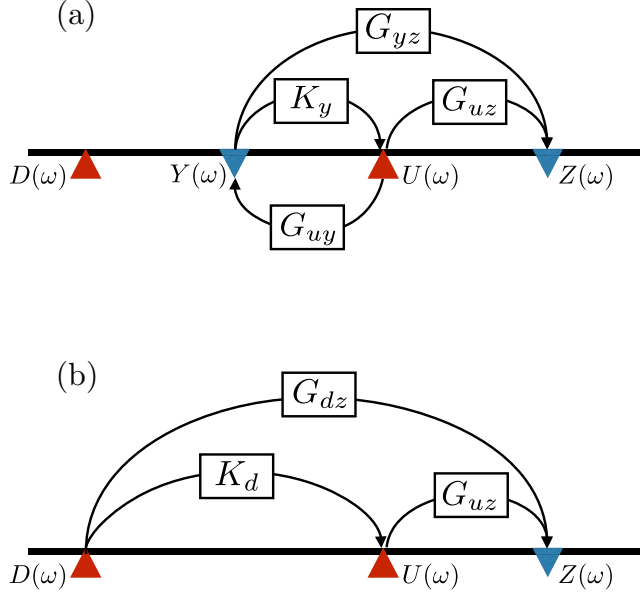


FIG. 3. Schematic of the inverse feedforward scheme showing the relative positions of the system inputs and outputs. The transfer functions between different elements are indicated, and the arrows indicate the direction where information is traveling. (a) Measurement-based control; (b) disturbance-based control.

turbulent jet in real time This simplified approach can be considered as an upper bound for control performance using flow sensors, as all of the information about the disturbances is available and taken into account by the control law, without observability issues. The results so obtained can then be compared to the control approach based on flow measurements. Figure 3 shows a simplified schematic of the inverse feedforward schemes obtained in measurement-based and disturbance-based approaches.

The jet was forced with band-limited stochastic signals in three different frequency bands: $0.3 \leq \text{St} \leq 0.45$, $0.3 \leq \text{St} \leq 0.65$, and $0.3 \leq \text{St} \leq 0.85$, where St is the Strouhal number, given by $\text{St} = fD/U_j$, with $f = \omega/(2\pi)$ the frequency. This Strouhal number range of forcing was selected based on the growth rates of disturbances computed through locally parallel linear stability analysis (LST) carried out in the initial jet region. The LST model assumes the flow to be homogeneous in the streamwise and azimuthal directions and in time, with flow disturbances of the form

$$q'(x, r, \theta, t) = \hat{q}(r)e^{i(\alpha x - \omega t)}e^{im\theta}, \quad (13)$$

where $q = [u_x, u_r, u_\theta, \rho, T]^T$ is a vector containing, respectively, the three components of velocity, density, and temperature, α and m are the wave numbers in the streamwise and azimuthal directions, respectively, and ω is the frequency. We also consider the Reynolds decomposition $q(x, r, \theta, t) = \bar{q}(x, r) + q'(x, r, \theta, t)$, where \bar{q} is the mean flow and q' is the fluctuation. Since here we consider forced axisymmetric wave packets, we compute the evolution of $m = 0$ disturbances only. Equation (13) and the Reynolds decomposition are introduced into the linearized Navier-Stokes equations written in cylindrical coordinates and linearized about the mean flow, as done by Tissot *et al.* [102]. Variations of the mean flow in the streamwise direction are neglected, following the locally parallel hypothesis. The linearized Navier-Stokes equations can then be written as a generalized eigenvalue problem,

$$\mathbf{L}\hat{q} = \alpha\mathbf{F}\hat{q}, \quad (14)$$

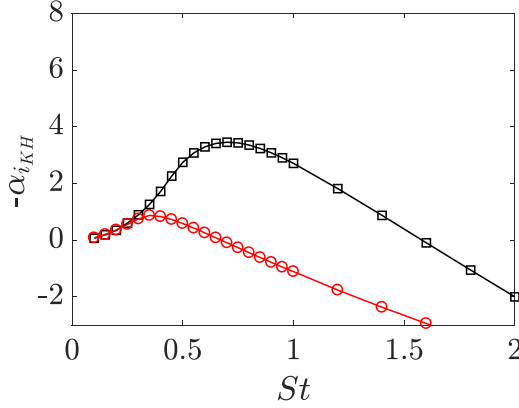


FIG. 4. Growth rate of the Kelvin-Helmholtz mode as a function of Strouhal number, computed through a locally parallel linear stability analysis carried out with velocity profiles measured at $x/D = 0.3$ (black squares) and $x/D = 2$ (red circles). Growth rates are shown with inverse sign, so that positive values mean exponential growth along positive x .

where α is the eigenvalue and \hat{q} the corresponding eigenvector. For a given Re and real ω , the evolution of the disturbances in the jet is governed by the sign of the imaginary part of the wave number, α_i : if $\alpha_i < 0$, the downstream-traveling disturbances will grow exponentially in the positive x direction. Details about the discretization of the velocity profiles and the linearized equations are given in Appendix B. For turbulent jets, the eigenspectrum in the initial region presents only one unstable mode, which is reminiscent of a Kelvin-Helmholtz-type instability. Figure 4 shows the growth rates of the unstable mode as a function of the Strouhal number, computed using mean velocity profiles measured close to the nozzle exit, at $x/D = 0.3$, and further downstream at $x/D = 2$. The stability model predicts exponential growth of disturbances over a broad range of Strouhal numbers going from $St = 0.1$ to $St = 1.5$ in the vicinity of the nozzle, with the highest growth rates occurring at $St \approx 0.7$. Further downstream, at the objective position, the growth rates are significantly reduced, but the jet still remains convectively unstable up to $St = 0.65$. Therefore, the range of forcing frequencies chosen for the control problem fall well within the range of the unstable zone of the spectrum.

This can be seen in Fig. 5, which shows the jet response to harmonic and stochastic forcing in different bandwidths. The signature of the forced disturbances is clearly seen in the power spectrum of velocity fluctuations at $x/D = 2$, showing that they have been amplified by the jet. We also note that the stochastic forcing leads to stochastic phases and amplitudes in the jet response, as opposed to harmonic forcing; this results in a time series which is more similar to what is seen in an unforced jet, as shown in Fig. 5. Hence the introduction of forcing simplifies the control tasks by enhancing axisymmetric disturbances, retaining nonetheless their stochastic nature. Such axisymmetric fluctuations can be sensed with the six-microphone ring array without significant spatial aliasing.

The transfer functions are identified empirically [62] in a preliminary open-loop step, by measuring the response of the jet to forcing and actuation separately. For the gain to be consistent with the disturbances one wishes to control, disturbance/objective, sensor/objective, and actuator/objective transfer functions should have the same frequency content. The transfer functions were computed using two kinds of disturbance signals: white noise and sine sweep; the results obtained were insensitive to the choice of signal. In what follows we report results using transfer functions obtained from bandpass filtered white noise.

Figure 6 shows frequency- and time-domain kernels obtained for a jet forced and actuated in the band $0.3 \leq St \leq 0.65$. We note that the frequency content of K_y and K_d is similar, although

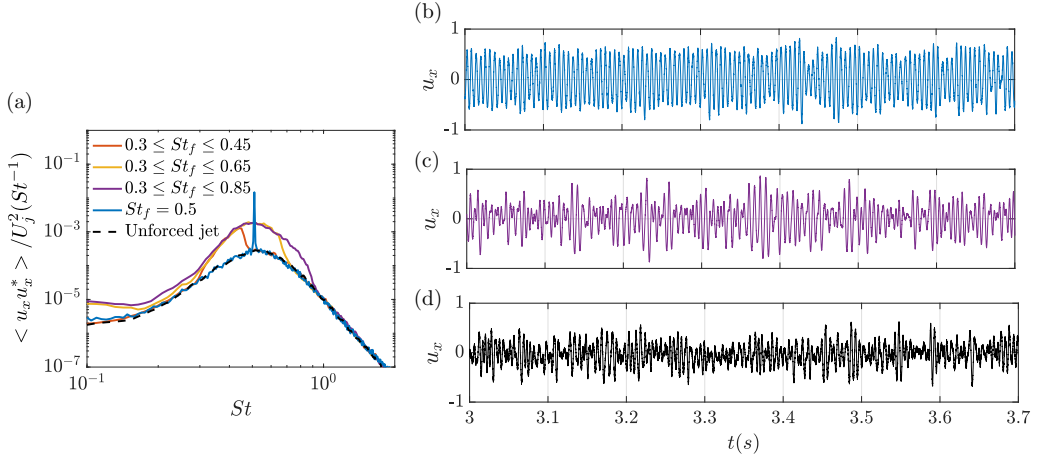


FIG. 5. Comparison of jet response to harmonic forcing at $St = 0.5$ and stochastic forcing in different bandwidths. (a) Power spectral density of velocity fluctuations measured at the jet centerline at $x/D = 2$. (b) Velocity fluctuation time signal of a jet forced harmonically; (c) velocity fluctuation time signal of a jet forced stochastically in the band $0.3 \leq St \leq 0.85$. (d) Velocity fluctuation time signal of an unforced jet. Velocity fluctuations have been normalized by their maximum values. Stochastic forcing produces stochastic phases and amplitudes in the response, similar to what is observed in the unforced jet.

the shape of K_y is flatter in the frequency band of interest. The time-domain kernels have a clear wavelike shape. There is significant damping of the oscillations in the k_y kernel due to the feedback transfer function, G_{uy} . The time shift between the k_y and k_d kernels is due to the fact that the sensors are downstream of the forcing system. Kernels obtained for the other two frequency bands of forcing and actuation (not shown) display similar behavior.

The control experiment is carried out using LabVIEW program equipped with a real-time module. The task of the software is to carry out the convolutions given by Eqs. (10) and (12) in real time, using unsteady signals from y or d , respectively, as input. The convolutions were carried out in a discrete form at a rate of 5 kHz, which has the maximum frequency allowed by the electronic hardware and CPU performance. The two methods explored here (d -based and y -based control)

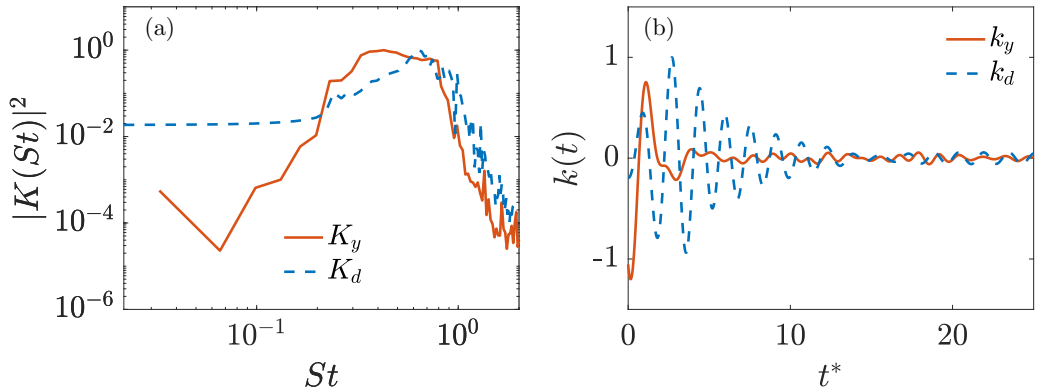


FIG. 6. Control kernels in (a) frequency and (b) time domain for a jet forced in the band $0.3 \leq St \leq 0.65$. The abscissa in (b) represent a nondimensional time, $t^* = tU_j/D$. Kernels are normalized by their maximum value for the sake of comparison.

have the same cost in terms of total power consumption necessary for actuation and control, and they seek to minimize the same objective. The only difference in their real-time operation is that in the y -based method the software performs the extra task of computing the coefficients of the Fourier series in the azimuthal direction using the signals from the six microphones. However, this extra operation was found to have negligible impact in terms of power and time consumption. The generation and acquisition of the time signals were made by a National Instruments PXIe-1071 card.

IV. RESULTS

A. Determination of linear behavior in jet response

Linearity is a key feature in the present control methodology, as is implicit in the linear superposition of Eq. (1). Here we use two-point coherence as a measure of the linearity of the system and a criterion for interpretation of the results. For a given pair of signals i and j , coherence is given as

$$\gamma_{ij}^2(\omega) = \frac{|\langle S_{ij}(\omega) \rangle|^2}{|\langle S_{ii}(\omega) \rangle| |\langle S_{jj}(\omega) \rangle|}, \quad (15)$$

where S_{ij} represents the CSD between i and j and S_{ii} and S_{jj} are the PSDs of each signal.

Control performance is underpinned by two kinds of coherence: the coherence between disturbance and objective, γ_{dz} , or between sensor and objective, γ_{yz} (depending on whether d or y are used as input to the control law), which dictate the accuracy of the estimation of the downstream evolution of disturbances, and the coherence between actuator and objective, γ_{uz} , which determines the accuracy of wave packet generation by the actuators. For small-amplitude disturbances applied to a laminar flow, such coherences are nearly unity due to the linear behavior of the flow [78]. However, for turbulent flows this is usually not the case, and in the present turbulent jet it is important to determine the linearity of flow responses. Earlier work shows that the jet response to plasma actuators has a significant degree of linearity [39]. We carry out here a related analysis, using the present actuators and sensors.

A careful preliminary study was carried out in open loop in order to determine the amplitude of the forcing, d , to use in the real-time experiment. For each forcing bandwidth tested, the jet response was measured at the objective position for increasing forcing amplitudes. Figure 7 illustrates typical response curves, obtained for stochastic forcing in the band $0.3 \leq \text{St} \leq 0.65$. For low forcing amplitudes, linear response regimes can be observed at different Strouhal numbers in the forcing bandwidth. Sufficiently high amplitudes can cause the response to saturate, as can be seen from the jet response at $\text{St} = 0.4$ and $\text{St} = 0.6$, which would cause an undesirable departure from the optimal scenario for linear control. The fact that the linear response regime for perturbations at $\text{St} = 0.3$ is sustained even for high forcing amplitudes is associated with the lower growth rates of disturbances in the lower limit of the forcing band, as predicted by the linear stability model (see Fig. 4). We have therefore selected the amplitudes so as to ensure that the jet response to forcing falls within linear regimes. A further motivation for using low-amplitude forcing is to avoid substantial changes to the jet dynamics compared to the unforced case.

B. Control results

1. Attenuation of velocity fluctuations at the objective position

With the amplitude of forcing d selected to ensure linear behavior, we obtained transfer functions and control kernels following the procedure described in Sec. III. The application of reactive control will now be studied.

Figure 8 shows PSDs of streamwise velocity fluctuations, u_x , measured in controlled and uncontrolled jets at the objective position. The results shown in Figs. 8(a), 8(c), and 8(e) were obtained using d as input, whereas those in Figs. 8(b), 8(d), and 8(f) were obtained using y as input. The spectra of the unforced jet is also shown for comparison. Two kinds of actuation

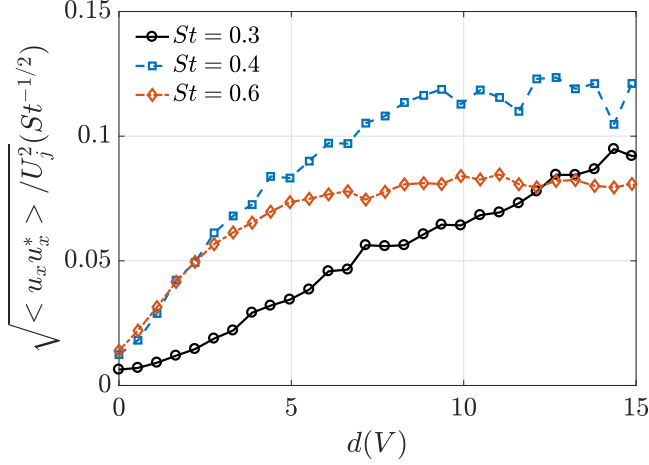


FIG. 7. Jet response to stochastic forcing in the band $0.3 \leq St \leq 0.65$ as a function of forcing amplitude. Response at three selected Strouhal numbers are shown. Amplitudes correspond to the voltage applied to the forcing system. For sufficiently low amplitudes, clear linear response regimes can be obtained at different Strouhal numbers within the forcing band. Response curves for other forcing bandwidths (not shown) displayed similar behavior.

were carried out: one whose gain was designed to reduce disturbance amplitudes, denoted $K_{y,d}^r$ [computed through Eqs. (10) and (12)] and another designed to amplify disturbances, $K_{y,d}^a$, obtained by applying a π phase shift to $K_{y,d}^r$. The superscripts r and a denote application of the reduction- and amplification-aimed kernels to the y -based and d -based control methods, respectively.

For the jet forced at the two narrowest frequency bands, control using the two methods (d based and y based) is effective in both reducing and amplifying the disturbances, demonstrating real-time control authority. It is also clear that the d -based control performs better than the y -based control. Indeed, in the K_r configuration the disturbances introduced in the jet are almost entirely eliminated. In the largest frequency band of forcing, $0.3 \leq St \leq 0.85$, control performance is degraded for both cases, and amplitudes could not be reduced to the unforced jet levels. Nonetheless, significant reductions are observed. Notice the use of a logarithmic scale in Fig. 7, with reductions attaining an order of magnitude in the favorable cases.

These trends can be understood in light of two-point coherences associated with the transfer functions. The control law is underpinned by estimation and actuation. In the estimation step, the downstream evolution of the disturbances is predicted as they reach the objective position. In this case, coherences γ_{dz} and γ_{yz} are the parameters that determine the accuracy of the estimation. In the actuation step, the incoming wave packets are eliminated by wave packets excited by the actuator with the correct phase and amplitude; the accuracy of this step is dictated by the values of γ_{uz} . Coherence values close to unity indicate a quasilinear behavior, which leads to accurate transfer functions; coherence loss, on the other hand, is associated with nonlinearity [2,77], and may result in poorly estimated objectives.

Figure 9 shows the behavior of the three important types of coherences as a function of St for the jet forced in different frequency bands. Within each frequency band, γ_{dz} is in general higher than γ_{yz} , especially at low Strouhal numbers. This is probably due to the fact that at low St the wave packets have lower growth rates and thus smaller amplitudes [103] in the initial jet region, which makes it harder to detect them through the sensors in the current setup. As the St increases and their amplitudes become bigger they become observable at the sensor position, and γ_{yz} becomes comparable to γ_{dz} . The lower observability at $St < 0.5$ results in worse estimation of the forced

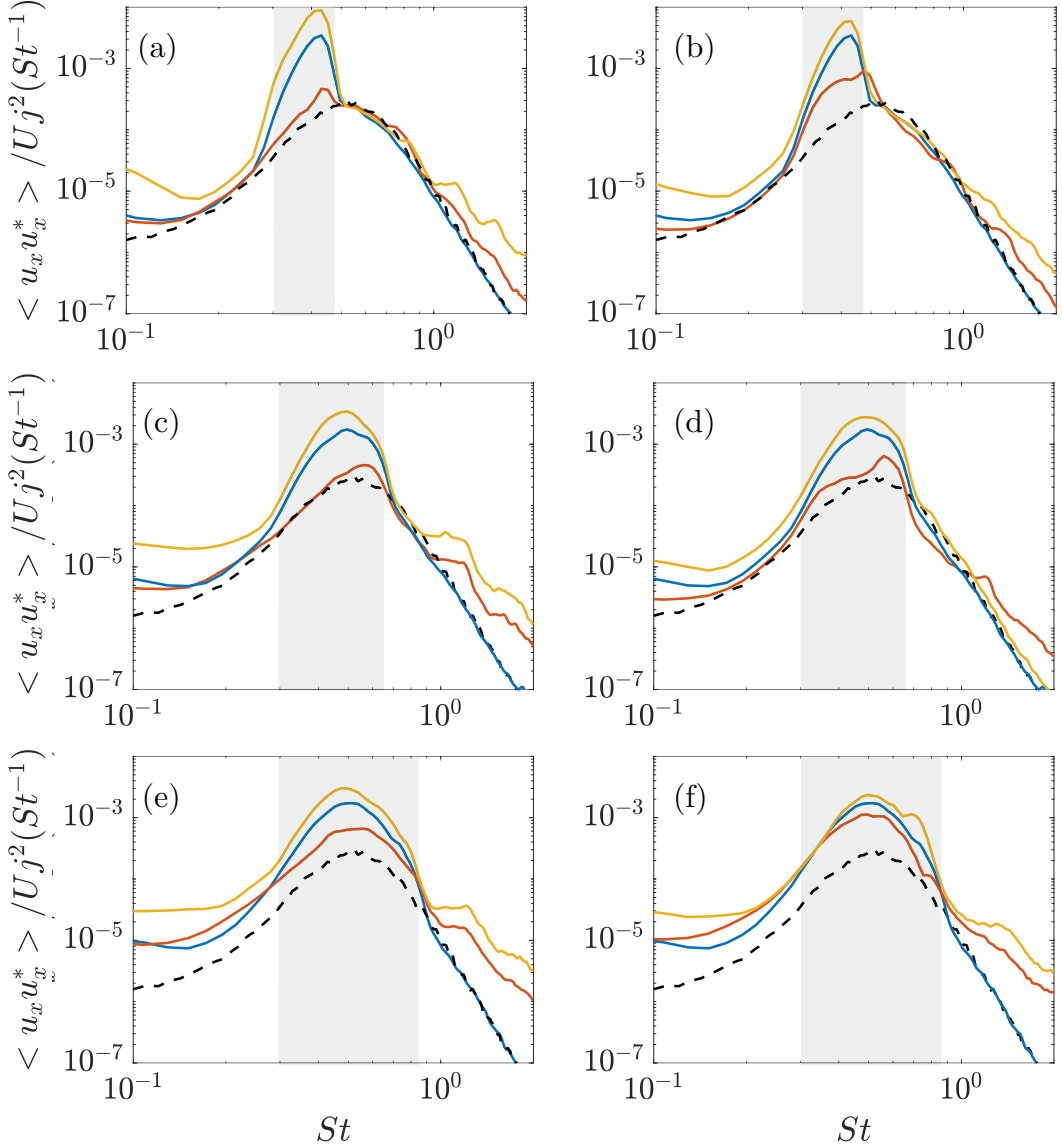


FIG. 8. Power spectral densities of streamwise velocity fluctuations, u_x , measured at the objective position ($x/D = 2$ at the centerline) of controlled and uncontrolled jets forced at three different bandwidths. —: baseline case (forced jet); —: controlled jet with reduction kernel, $K_{y,d}^r$; —: controlled jet with amplification kernel, $K_{y,d}^a$; - - -: unforced jet. (a),(c),(e) Control based on the external disturbances, d , as input to the control law; (b),(d),(f) control based on flow measurements, y , as input to the control law. Forcing bandwidths, represented by the gray shaded areas, are $0.3 \leq St \leq 0.45$, $0.3 \leq St \leq 0.65$, and $0.3 \leq St \leq 0.85$.

disturbances, which explains to a great extent the inferior performance in comparison with the d -based control.

This issue could, in principle, be mitigated by moving the sensors downstream, where wave packet amplitudes are higher. This, however, has the associated side effect of increasing sensor acoustic contamination by the actuators, which might become excessively high, hindering estimation. Moving the entire setup downstream (but keeping the same relative distances between

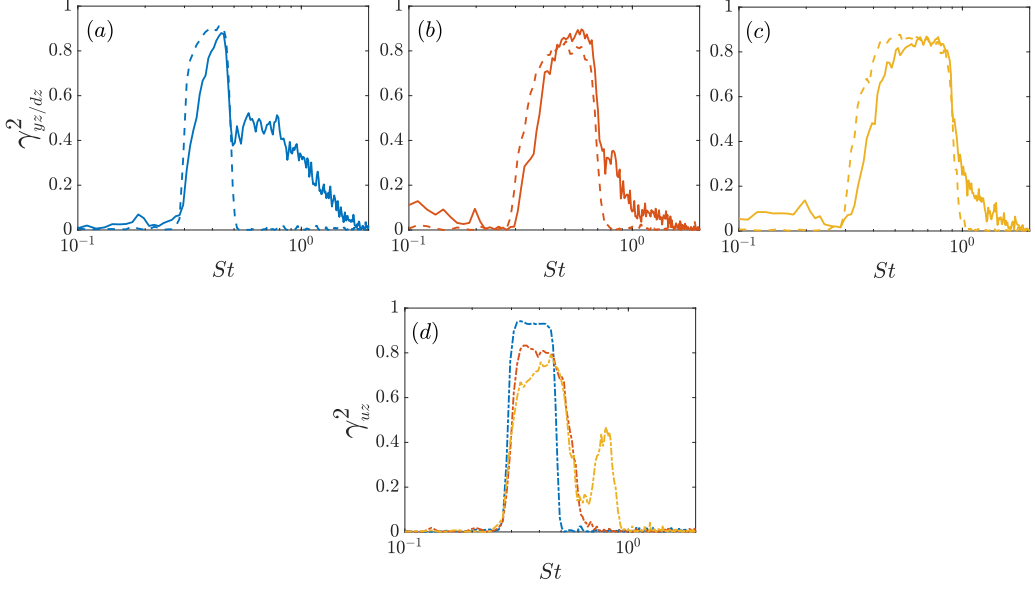


FIG. 9. Coherences associated to the control results shown in Fig. 8. (a)–(c) Comparison between sensor/objective (solid line), γ_{yz} , and disturbance/objective (dashed line), γ_{dz} , coherences measured with increasing frequency bands of forcing. (d) Actuator/objective coherences, γ_{uz} , measured for different actuation frequency bands. The color code for frequency band is the following: —: $0.3 \leq St \leq 0.45$; —: $0.3 \leq St \leq 0.65$; —: $0.3 \leq St \leq 0.85$.

sensors and actuators), on the other hand, is not an appealing solution, since the linear evolution of disturbances, upon which the present control strategy is based, only holds in a limited initial region of the jet development. The present setup was the best compromise found given the experimental constraints. Optimizing sensor and actuator placement is something to be considered in future work.

We also observe in Fig. 9(d) that, with increasing frequency bands of forcing, there is a severe drop in γ_{uz} . This may be associated with two issues: the first is that the jet response to actuation may be nonlinear; the second issue is that actuators are placed outside of the region of nonzero mean flow. Therefore, in order to produce an actuation signal with amplitudes sufficient to eliminate the disturbances introduced upstream, one is obliged to increase amplitudes past the linear zone, triggering nonlinear actuator behavior. Regardless of the precise cause, coherence loss due to nonlinearity becomes more prominent at the higher frequency band of actuation and leads to the degradation of control performance seen in Figs. 8(e) and 8(f).

We also note that low frequency disturbances ($St < 0.3$) are also amplified by the jet, as can be seen in Figs. 5 and 8, even though the jet is not directly forced at those frequencies. This suggests that there is some degree of nonlinear interactions occurring, in spite of the attempts to keep nonlinear amplification to a minimum. The precise cause of this phenomenon is still under investigation. However, we emphasize that the linearity assumption holds in the Strouhal number range where the control kernels are designed (as observed by the linear portion of the curves shown in Fig. 7 and the high coherences reported in Fig. 9), guaranteeing control performance.

C. Control effect downstream of the objective position

We also investigated the effect of the control on the downstream evolution of the forced wave packets beyond the objective position. Figure 10 shows streamwise velocity spectra at the jet center line and radial profiles of streamwise rms velocity, u'_x , of uncontrolled and controlled jets, measured at three positions downstream of the objective. Forcing was applied in the band $0.3 \leq St \leq 0.45$ and

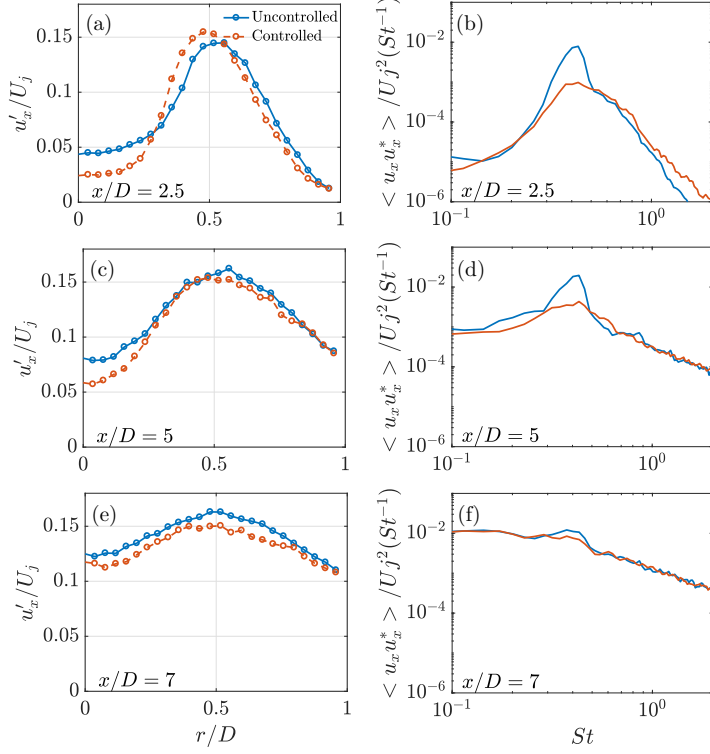


FIG. 10. Effect of control downstream of the objective position. (a),(c),(e) Radial profiles of streamwise rms velocity; (b),(d),(f) power spectral densities of streamwise velocity fluctuation measured at the jet centerline. The uncontrolled case corresponds to the baseline jet, forced in the bandwidth $0.3 \leq St \leq 0.45$, and the controlled case was obtained with a reduction-aimed kernel, K_d^r .

control was carried out with the K_r kernel with d as input. The difference between uncontrolled and controlled jets is clear in the spectra and in rms levels up to $x/D = 7$. Close to the objective position, rms reduction is restricted to radial positions close to the jet axis, and an amplification effect occurs at $0.25 \leq r/D \leq 0.5$. This undesired phenomenon is associated with high-frequency content (likely due to small eddies generated by penetration of the actuation jets into the flow) close to the objective position, as can be seen in the spectra of Fig. 8. However, these scales gradually lose energy as they evolve downstream, since the jet is convectively stable at this position for $St > 0.7$, as can be seen in Fig. 4. Therefore, further downstream the desired trend of reduction is obtained across the shear layer. The results show that, even though the control strategy has a localized character insofar as it is formulated to achieve its objective at a specific position within the jet, it produces reductions of wave packet amplitudes throughout the jet.

V. CONCLUSIONS

We have presented an experimental study of real-time, reactive control of stochastic disturbances in forced turbulent jets. The control framework is based on linear destructive interference, and it is motivated by the recent success of this approach to control Tollmien-Schlichting waves [63,78] in a laminar boundary layer and Kelvin-Helmholtz instabilities in transitional mixing layers [64]. We also build on numerous previous studies that have established the possibility of exciting turbulent jets at different frequencies [14–21,25–27,29–31,33–35,38,39,86,87]. Here we use this fact to derive

our control law. But, unlike those previous studies, we consider a framework in which broadband disturbances can be manipulated in real time through reactive control.

The control law is given in terms of transfer functions identified empirically through a system identification technique. This is done by measuring the jet response to stochastic forcing at the nozzle lip, stochastic actuation at $x/D = 1.5$, and velocity measurements at $x/D = 2$. This setup, with actuation computed in real time using measurements done upstream, results in an inverse feedforward scheme [64,64], which is suitable for amplifier flows [57]. One of the advantages of the present approach with respect to optimal linear schemes, such as LQG and LQR, is that it is conceptually simpler and provides a clear physical interpretation of the control mechanism: it should correspond to a destructive interference pattern between incoming wave packets and wave packets generated by the actuators. Here we only explore the mentioned inverse feedforward scheme, which has been shown previously to produce the best performance for amplifier flows, but also to suffer from lack of robustness in the presence of undesirable or unmodeled disturbances [100]. Improving control robustness through feedback and adaptive strategies is an interesting future direction.

The forcing at the nozzle lip produces axisymmetric wave packets with stochastic phases and amplitudes, similar to turbulent fluctuations that exist in unforced jets. We have demonstrated that control of such stochastic disturbances is possible in a turbulent jet. Reductions of an order of magnitude are obtained in velocity spectra on the jet center line. The attenuation of the disturbances is found to persist over an extended streamwise region downstream of the objective position. This shows the potential of the present control strategy to provide global reductions of unsteady disturbances.

Working with a forced jet was a necessary and fundamental first step for the longer-term objective of reactive control of an unforced jet. The latter problem requires a more refined choice of sensors and their positioning in order to avoid azimuthal aliasing issues, and the design of better actuators in order to avoid nonlinear actuator behavior, as shown in Fig. 9 as the frequency band of actuation is increased. The performance of the control is shown to be largely underpinned by coherences between sensor and objective, on one hand, and actuator and objective on the other. The high coherences obtained at the narrower forcing bandwidths imply that the linear mechanisms of wave packet dynamics are not substantially altered by the forcing [14,15] and remain much the same as in unforced jets. Therefore, the present control strategy can, in principle, work in the unforced jet provided that the coherence metrics are used to guide optimization of sensor and actuator placement. Current hardware constraints limited the application of the experiment to a low-Mach-number jet. It still remains to be seen whether the present control strategy will eventually lead to an effective jet-noise reduction. Nevertheless, the demonstrated success in canceling axisymmetric wave packets, and the recognized importance of these to sound radiation [1,2], gives hope that one can obtain meaningful reductions in higher-Mach-number jets.

ACKNOWLEDGMENTS

I.A.M. acknowledges support from the Science Without Borders program, CNPq Grant No. 200676/2015-6. E.M. acknowledges support from CAPES Grant No. 88881.190271/2018-01. P.J., A.V.G.C., and F.J.S. acknowledge support from the CAPES Science Without Borders Project No. A073/2013. The authors are indebted to R. Kari and D. Eysseric for their invaluable work during the experimental campaign. We also wish to thank V. Jaunet and S. Piantanida for their help on the design of the real-time module and on the first estimation and control attempts.

APPENDIX A: TRANSFER FUNCTIONS

In this Appendix we compare the typical transfer functions of the control system, G_{yz} , G_{uz} , and G_{uy} . Figure 11 shows the amplitudes and phases of the transfer functions computed by forcing the jet in the frequency band $0.3 \leq St \leq 0.65$. The variation of the phases with Strouhal number reveals the nature of the perturbations modeled by the transfer functions. The phases of G_{yz} and G_{uz}

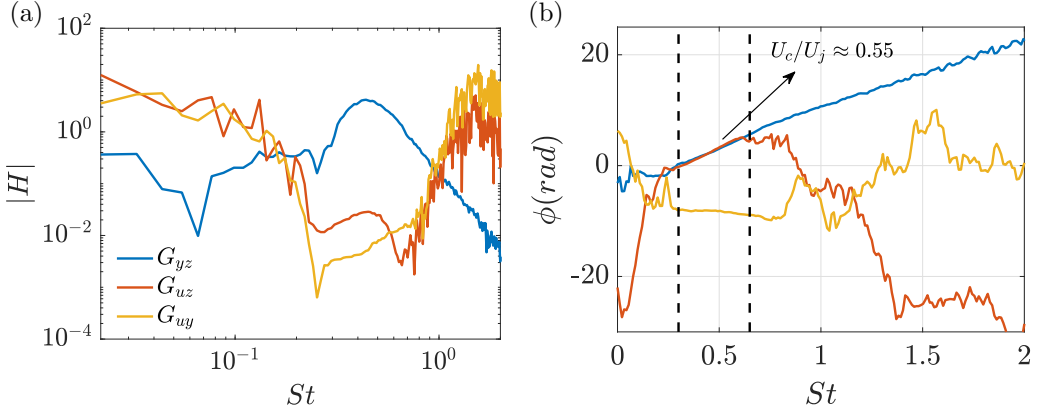


FIG. 11. Amplitudes (a) and phases (b) of the system transfer functions. The black dashed lines delimit the frequency band of forcing and actuation, $0.3 \leq St \leq 0.65$. The mean phase speed (averaged in the frequency band of forcing) of the hydrodynamic perturbation is indicated.

increase linearly with Strouhal number, with phase velocities typical of dispersive hydrodynamic wave packets. The phase of G_{uy} , on the other hand, is practically constant in the frequency band of actuation, consistent with an acoustic signature. Therefore, the inclusion of G_{uy} in the expression for the control kernel accounts only for an acoustic contamination.

APPENDIX B: LOCALLY PARALLEL LINEAR STABILITY ANALYSIS

The linearized Navier-Stokes equations for axisymmetric ($m = 0$) disturbances are given by

$$\begin{aligned}
 -i\omega \hat{u}_x + i\alpha \bar{U}_x \hat{u}_x + \hat{u}_r \bar{U}'_x = & -\frac{\gamma-1}{\gamma} i\alpha \hat{T} - \frac{\gamma-1}{\gamma} \frac{\bar{T}}{\bar{\rho}} i\alpha \hat{\rho} + \frac{1}{\bar{\rho} \text{Re}} \left\{ \bar{\mu} \left[-\alpha^2 \hat{u}_x + \frac{1}{r} \frac{\partial}{\partial r} \left(r \frac{\partial \hat{u}_x}{\partial r} \right) \right] \right. \\
 & + \frac{\bar{\mu}}{3} \left(-\alpha^2 \hat{u}_x + i\alpha \frac{\partial \hat{u}_r}{\partial r} + \frac{i\alpha}{r} \hat{u}_r \right) + \frac{\partial \bar{\mu}}{\partial r} \left(i\alpha \hat{u}_r + \frac{\partial \hat{u}_x}{\partial r} \right) \\
 & \left. + \frac{\mu}{r} \frac{\partial}{\partial r} \left(r \frac{\partial \bar{U}_x}{\partial r} \right) \frac{\partial \mu}{\partial r} \frac{\partial \bar{U}_x}{\partial r} \right\}, \tag{B1}
 \end{aligned}$$

$$\begin{aligned}
 -i\omega \hat{u}_r + i\alpha \bar{U}_x \hat{u}_r = & -\frac{\gamma-1}{\gamma} \frac{\partial \hat{V}}{\partial r} - \frac{\gamma-1}{\gamma} \frac{\bar{T}}{\bar{\rho}} \frac{\partial \hat{\rho}}{\partial r} - \frac{\gamma-1}{\gamma} \frac{\hat{\rho}}{\bar{\rho}} \frac{\partial \bar{T}}{\partial r} - \frac{\gamma-1}{\gamma} \frac{\hat{T}}{\bar{\rho}} \frac{\partial \bar{\rho}}{\partial r} \\
 & + \frac{1}{\bar{\rho} \text{Re}} \left\{ \bar{\mu} \left[-\alpha^2 \hat{u}_r + \frac{1}{r} \frac{\partial}{\partial r} \left(r \frac{\partial \hat{u}_r}{\partial r} \right) \right] \right. \\
 & - \frac{\bar{\mu} \hat{u}_r}{r^2} + i\alpha \mu \bar{U}'_x + \frac{\bar{\mu}}{3} \left(i\alpha \frac{\partial \hat{u}_x}{\partial r} + \frac{\partial^2 \hat{u}_r}{\partial r^2} + \frac{1}{r} \frac{\partial \hat{u}_r}{\partial r} - \frac{\hat{u}_r}{r^2} \right) \\
 & \left. + \frac{\partial \bar{\mu}}{\partial r} \left(2 \frac{\partial \hat{u}_r}{\partial r} - \frac{2}{3} i\alpha \hat{u}_x - \frac{2}{3} \frac{\partial \hat{u}_r}{\partial r} - \frac{2}{3} \frac{\hat{u}_r}{r} \right) \right\}, \tag{B2}
 \end{aligned}$$

$$\begin{aligned}
 -i\omega \hat{T} + \hat{u}_r \frac{\partial \bar{T}}{\partial r} + i\alpha \bar{U}_x \hat{T} + (\gamma-1) \bar{T} \left(i\alpha \hat{u}_x + \frac{\partial \hat{u}_r}{\partial r} + \frac{\partial \hat{u}_r}{\partial r} \right) \\
 = \frac{\gamma}{\bar{\rho} \text{Re Pr}} \left[\bar{\mu} \left(-\alpha^2 \hat{T} + \frac{\partial^2 \hat{T}}{\partial r^2} + \frac{1}{r} \frac{\partial \hat{T}}{\partial r} \right) + \frac{\partial \bar{\mu}}{\partial r} \frac{\partial \hat{T}}{\partial r} \right]
 \end{aligned}$$

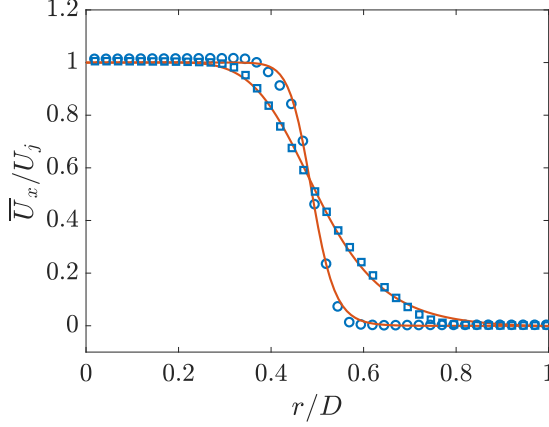


FIG. 12. Experimental and fitted mean flow profiles. The circles correspond to mean experimental profiles measured at $x/D = 0.3$ and the squares correspond to measurements at $x/D = 2$. The solid lines are the fitted profiles.

$$+ \frac{\partial \mu}{\partial r} \frac{\partial \bar{T}}{\partial r} + \mu \left(\frac{\partial^2 \bar{T}}{\partial r^2} + \frac{1}{r} \frac{\partial \bar{T}}{\partial r} \right) + \frac{\gamma}{\bar{\rho}} \left[\frac{\mu}{\text{Re}} \left(\frac{\partial \bar{U}_x}{\partial r} \right)^2 + \frac{2\bar{\mu}}{\text{Re}} \frac{\partial \bar{U}_x}{\partial r} \left(i\alpha \hat{u}_r + \frac{\partial \hat{u}}{\partial r} \right) \right], \quad (\text{B3})$$

$$-i\omega \hat{p} + i\alpha \bar{U}_x \hat{p} + \bar{\rho} i\alpha \hat{u} + \bar{\rho} \frac{\partial \hat{v}}{\partial r} + \hat{v} \frac{\partial \bar{\rho}}{\partial r} + \frac{\bar{\rho} \hat{v}}{r} = 0, \quad (\text{B4})$$

for x momentum, r momentum, energy, and continuity, respectively. The hats denote Fourier transformed quantities. The mean fields of temperature and density are determined using the Crocco-Busemann relation and the perfect gas law. The viscosity, $\bar{\mu}$, is determined using Sutherland's law. The coefficients are then rearranged in matrices **L** and **F** shown in Eq. (14) to yield an eigenvalue problem. Viscous terms containing α^2 terms were neglected, due to the high Reynolds number of the flow, following Rodríguez *et al.* [104]. Dirichlet boundary conditions are used for a far-field boundary located at $r/D = 10^3$ and the radial direction is discretized using Chebyshev collocation points. 400 Chebyshev points were found to be sufficient to obtain a converged eigen-spectrum. The system (14) can then be solved for different frequencies and streamwise locations. At each location the mean flow profiles were fitted with the following function:

$$U_{fit}/U_j = 0.5 \left(1 + \{1 + c[1 - \tanh(r)^2]\} \left[1 + d \left(\frac{1}{\cosh(r)} \right)^2 \right] \times \tanh \left\{ b \left[\left(\frac{0.5 + a}{r} \right) - \left(\frac{r}{0.5 + a} \right) \right] \right\} \right), \quad (\text{B5})$$

where a , b , c , and d are constants that have been found through a nonlinear least square algorithm. Figure 12 shows examples of experimental and fitted mean velocity profiles at $x/D = 0.3$ and $x/D = 2$.

-
- [1] P. Jordan and T. Colonius, Wave packets and turbulent jet noise, *Annu. Rev. Fluid Mech.* **45**, 173 (2013).
 - [2] A. V. G. Cavalieri, P. Jordan, and L. Lesshafft, Wave-packet models for jet dynamics and sound radiation, *Appl. Mech. Rev.* **71**, 020802 (2019).
 - [3] M. J. Lighthill, On sound generated aerodynamically I. General theory, *Proc. R. Soc. London A* **211**, 564 (1952).

- [4] N. H. Sayed, K. L. Mikkelsen, and J. E. Bridges, Acoustics and thrust of separate-flow exhaust nozzles with mixing devices for high-bypass-ratio engines, in *Proceedings of the 6th Aeroacoustics Conference and Exhibit* (2012).
- [5] M. Samimy, K. Zaman, and M. Reeder, Effect of tabs on the flow nad noise field of an axisymmetric jet, *AIAA J.* **31**, 609 (1993).
- [6] J. E. Bridges and C. A. Brown, Parametric testing of chevrons on single flow hot jets, in *Proceedings of the 10th AIAA/CEAS Aeroaroustics Conference*, No. 2824 (AIAA, Reston, VA, 2004).
- [7] K. Zaman, J. Bridges, and D. Huff, Evolution from “tabs” to “chevron” technology-a review, *Int. J. Aeroacoustics* **10**, 685 (2011).
- [8] K. B. Zaman, M. F. Reeder, and M. Samimy, Control of axisymmetric jet using vortex generators, *Phys. Fluids* **6**, 778 (1994).
- [9] V. Mingle, Optimization of lobe mixer geometry and nozzle length for minimum jet noise, in *Proceedings of the 6th Aeroacoustics Conference and Exhibit* (2012).
- [10] K. Viswanathan, M. Shur, P. Spalart, and M. Strelets, Flow and noise predictions for single and dual-stream beveled nozzles, *AIAA J.* **46**, 601 (2008).
- [11] M. B. Alkislar, A. Krothapalli, and G. W. Butler, The effect of streamwise vorticity on the aeroacoustics of a Mach 0.9 jet, *J. Fluid Mech.* **578**, 139 (2007).
- [12] A. Sinha, K. Gudmundsson, H. Xia, and T. Colonius, Parabolized stability analysis of jets from serrated nozzles, *J. Fluid Mech.* **789**, 36 (2016).
- [13] F. C. Lajús, A. V. G. Cavalieri, C. J. Deschamps, and T. Colonius, Spatial stability analysis of subsonic corrugated jets, *J. Fluid Mech.* **876**, 766 (2019).
- [14] S. Crow and F. Champagne, Orderly structure in jet turbulence, *J. Fluid Mech.* **48**, 547 (1971).
- [15] C. J. Moore, The role of shear-layer instability waves in jet exhaust noise, *J. Fluid Mech.* **80**, 321 (1977).
- [16] D. Bechert and E. Pfizenmaier, On the amplification of broadband jet noise by a pure tone excitation, *J. Sound Vib.* **43**, 581 (1975).
- [17] V. Kibens, On the role of vortex pairing in jet noise generation, in *Proceedings of the Joint Symposium, Goettingen, West Germany, August 28–31, 1979 (A80-23890 08-71)* Springer-Verlag, Berlin, 1979), pp. 174–180.
- [18] G. L. Morrison and D. K. McLaughlin, Noise generation by instabilities in low Reynolds number supersonic flows, *J. Sound Vib.* **65**, 177 (1979).
- [19] M. Favre-Marinet and G. Binder, Structure of pulsating jets, *J. de Mécanique* **18**, 355 (1979).
- [20] B. Jubelin, New experimental studies on jet noise amplification, in *Proceedings of the 6th Aeroacoustics Conference and Exhibit* (1980).
- [21] K. B. M. Q. Zaman and A. K. M. F. Hussain, Turbulence suppression in free shear flows by controlled excitation, *J. Fluid Mech.* **103**, 133 (1981).
- [22] A. K. M. F. Hussain and K. B. M. Q. Zaman, Vortex pairing in a circular jet under controlled excitation. Part 1: General jet response, *J. Fluid Mech.* **101**, 449 (1980).
- [23] A. K. M. F. Hussain and K. B. M. Q. Zaman, Vortex pairing in a circular jet under controlled excitation. Part 2: Coherent structure dynamics, *J. Fluid Mech.* **101**, 493 (1980).
- [24] J. Laufer and T.-C. Yen, Noise generation by a low-Mach-number jet, *J. Fluid Mech.* **134**, 1 (1983).
- [25] C. M. Ho and P. Huerre, Perturbed free shear-layers, *Annu. Rev. Fluid Mech.* **16**, 365 (1984).
- [26] S. Raghu, B. Lehmann, and P. A. Monkewitz, On the mechanism of “Sidejet” generation in periodically excited axisymmetric jets, in *Advances in Turbulence 3: Proceedings of the Third European Turbulence Conference Stockholm*, edited by A. V. Johansson and P. H. Alfredsson (Springer, Berlin, Heidelberg, 1990).
- [27] R. A. Petersen and T. A. Long, Controlled interactions in a forced axisymmetric jet. Part 2. The modulation of broadband turbulence, *J. Fluid Mech.* **235**, 57 (1991).
- [28] B. Henderson, Fifty years of fluidic injection for jet noise reduction, *Int. J. Aeroacoustics* **9**, 91 (2010).
- [29] V. H. Arakeri, A. Krothapalli, V. Siddavaram, M. B. Alkislar, and L. M. Lourenco, On the use of microjets to suppress turbulence in a Mach 0.9 axisymmetric jet, *J. Fluid Mech.* **490**, 75 (2003).
- [30] A. Krothapalli, L. Venkatakrishnan, L. Lourenco, B. Greska, and R. Elavasaran, Turbulence and noise suppression of a high-speed jet by water injection, *J. Fluid Mech.* **491**, 131 (2003).

- [31] B. Greska, A. Krothapalli, N. Burnside, and W. C. Horne, High-speed jet noise reduction using microjets on a jet engine, *AIAA J.* **2004**, 2969 (2004).
- [32] T. Castelain, M. Sunyach, D. Juvé, and J. C. Béra, Jet noise reduction by impinging microjets: An aerodynamic investigation testing microjet parameters, *AIAA J.* **2007**, 3419 (2007).
- [33] E. Calvo, J. L. Santoloya J. A. García, and L. Aísa, Measurements about the air motion in an acoustically forced jet: effects of the dispersed phase on the coherent flow structure, *Exp. Fluids* **55**, 1635 (2014).
- [34] A. Sinha, A. Towne, T. Colonius, R. H. Schlinker, R. Reba, J. C. Simonich, and D. W. Shannon, Active control of noise from hot supersonic jets, *AIAA J.* **56**, 933 (2018).
- [35] J. B. Freund and P. Moin, Jet mixing enhancement by high-amplitude fluidic actuation, *AIAA J.* **38** (2000).
- [36] M. Samimy, I. Adamovich, B. Webb, J. Kastner, J. Hileman, S. Keshav, and P. Palm, Development and characterization of plasma actuators for high-speed jet control, *Exp. Fluids* **37**, 577 (2004).
- [37] Y. G. Utkin, S. Keshav, J.-H. Kim, J. Kastner, I. V. Adamovich, and M. Samimy, Development and use of localized arc-filament plasma actuators for high-speed control, *J. Phys. D* **40**, 685 (2007).
- [38] M. Samimy, M. Debiassi, E. Caraballo, A. Serrani, X. Yuan, J. Little, and J. Myatt, Feedback control of subsonic cavity flows using reduced-order models, *J. Fluid Mech.* **579**, 315 (2007).
- [39] A. Sinha, H. Alkandry, M. Kearney-Fischer, M. Samimy, and T. Colonius, The impulse response of a high-speed jet forced with localized arc filament plasma, *Phys. Fluids* **24**, 125104 (2012).
- [40] J. Kühnen, B. Song, D. Scarselli, N. B. Budanur, M. Riedl, A. P. Willis, and B. Hof, Destabilizing turbulence in pipe flow, *Nat. Phys.* **14**, 386 (2018).
- [41] N. Fabbiane, B. Simon, F. Fischer, S. Grundmann, S. Bagheri, and D. Henningson, On the role of adaptivity for robust laminar flow control, *J. Fluid Mech.* **767**, R1 (2015).
- [42] C. Cossu and J. M. Chomaz, Global Measures of Local Convective Instabilities, *Phys. Rev. Lett.* **78**, 4387 (1997).
- [43] T. R. Bewley, Flow control: New challenges for a new renaissance, *Prog. Aerosp. Sci.* **37**, 21 (2001).
- [44] J. Kim and T. T. Bewley, A linear systems approach to flow control, *Annu. Rev. Fluid Mech.* **39**, 383 (2007).
- [45] P. Moin and T. R. Bewley, Feedback control of turbulence, *Appl. Mech. Rev.* **47**, S3 (1994).
- [46] S. S. Joshi, J. L. Speyer, and J. Kim, A systems theory approach to the feedback stabilization of infinitesimal and finite-amplitude disturbances in plane Poiseuille flow, *J. Fluid Mech.* **332**, 157 (1997).
- [47] M. Högberg, T. R. Bewley, and D. Henningson, Linear feedback control and estimation of transition in plane channel flow, *J. Fluid Mech.* **481**, 149 (2003).
- [48] M. Chevalier, J. Hoepffner, E. Åkervik, and D. Henningson, Linear feedback control and estimation applied to instabilities in spatially developing boundary layers, *J. Fluid Mech.* **588**, 163 (2007).
- [49] D. G. Crighton and M. Gaster, Stability of slowly diverging jet flow, *J. Fluid Mech.* **77**, 397 (1976).
- [50] B. J. McKeon and A. S. Sharma, A critical-layer framework for turbulent pipe flow, *J. Fluid Mech.* **658**, 336 (2010).
- [51] S. Bagheri, D. S. Henningson, J. Hoepffner, and P. J. Schmid, Input-output analysis and control design applied to a linear model of spatially developing flows, *Appl. Mech. Rev.* **62**, 020803 (2009).
- [52] E. Åkervik, J. Hoepffner, U. Eherenstien, and D. S. Henningson, Optimal growth, model reduction and control in a separated boundary-layer flow using global eigenmodes, *J. Fluid Mech.* **579**, 305 (2007).
- [53] A. Barbagallo, D. Sipp, and P. Schmid, Closed-loop control of an open cavity flow using reduced-order models, *J. Fluid Mech.* **641**, 1 (2009).
- [54] A. Barbagallo, G. Dergham, D. Sipp, P. J. Schmid, and J. C. Robinet, Closed-loop control of unsteadiness over a rounded backward-facing step, *J. Fluid Mech.* **703**, 326 (2012).
- [55] D. Sipp, O. Marquet, P. Meliga, and A. Barbagallo, Dynamics and control of global instabilities in open-flows: A linearized approach, *Appl. Mech. Rev.* **63**, 030801 (2010).
- [56] D. Sipp and P. J. Schmid, Linear closed-loop control of fluid instabilities and noise-induced perturbations: A review of approaches and tools, *Appl. Mech. Rev.* **68**, 020801 (2016).
- [57] P. J. Schmid and D. Sipp, Linear control of oscillator and amplifier flows, *Phys. Rev. Fluids* **1**, 040501 (2016).

- [58] P. J. Schmid and D. S. Henningson, Optimal energy density growth in Hagen-Poiseuille flow, *J. Fluid Mech.* **277**, 197 (1994).
- [59] N. Fabbiane, O. Semeraro, S. Bagheri, and D. S. Henningson, Adaptive and model-based control theory applied to convectively unstable flows, *Appl. Mech. Rev.* **66**, 060801 (2014).
- [60] E. Laurien and L. Kleiser, Numerical simulation of boundary-layer transition and transition control, *J. Fluid Mech.* **199**, 403 (1989).
- [61] Y. Li and M. Gaster, Active control of boundary-layer instabilities, *J. Fluid Mech.* **550**, 185 (2006).
- [62] K. Sasaki, S. Piantanida, A. V. G. Cavalieri, and P. Jordan, Real-time modelling of wavepackets in jets, *J. Fluid Mech.* **821**, 458 (2017).
- [63] K. Sasaki, P. Morra, N. Fabbiane, A. V. G. Cavalieri, A. Hanifi, and D. Henningson, On the wave-cancelling nature of boundary layer flow control, *Theor. Comput. Fluid Dyn.* **32**, 593 (2018).
- [64] K. Sasaki, G. Tissot, A. V. G. Cavalieri, F. J. Silvestre, P. Jordan, and D. Biau, Closed-loop control of a free shear flow: a framework using the parabolized stability equations, *Theor. Comput. Fluid Dyn.* **32**, 765 (2018).
- [65] H. Tol, C. de Visser, and M. Kotsonis, Experimental model-based estimation and control of natural Tollmien-Schlichting waves, *AIAA J.* **57**, 1 (2019).
- [66] L. Ljung, *System Identification: Theory for the User*, 2nd ed. (Prentice Hall, Englewood Cliffs, NJ, 1998).
- [67] S.-C. Huang and J. Kim, Control and system identification of a separated flow, *Phys. Fluids* **20**, 101509 (2008).
- [68] A. Hervé, D. Sipp, P. J. Schmid, and M. Samuelides, A physics-based approach to flow control using system identification, *J. Fluid Mech.* **702**, 26 (2012).
- [69] R. Rathnasingham and K. Breuer, Active control of turbulent boundary layers, *J. Fluid Mech.* **495**, 209 (2003).
- [70] R. Erdmann, A. Pätzold, M. Engert, I. Peltzer, and W. Nitsche, On active control of laminar-turbulent transition on two-dimensional wings, *Philos. Trans. R. Soc. London* **369**, 1382 (2011).
- [71] F. Juillet, B. McKeon, and P. Schmid, Experimental control of natural perturbations in channel flow, *J. Fluid Mech.* **752**, 296 (2014).
- [72] L. Cattafesta, Q. Song, D. R. Williams, C. W. Rowley, and F. S. Alvi, Active control of flow-induced cavity oscillations, *Prog. Aerosp. Sci.* **44**, 479 (2008).
- [73] L. N. Cattafesta III, S. Garg, M. Choudhari, and F. Li, Active control of flow-induced cavity resonance, *AIAA J.* **1997**, 1804 (1997).
- [74] D. R. Williams, C. Rowley, T. Colonius, R. M. Murray, D. MacMartin, and D. Fabris, Model-based control of cavity oscillations - Part 1: Experiments, *AIAA J.* **2002**, 0972 (2002).
- [75] R. H. Cabell, M. A. Kegerise, D. E. Cox, and G. P. Gibbs, Experimental feedback control of flow-induced cavity tones, *AIAA J.* **44**, 1807 (2006).
- [76] M. Debiasi and M. Samimy, Logic-based active control of subsonic cavity flow resonance, *AIAA J.* **42**, 1901 (2004).
- [77] A. V. G. Cavalieri and A. Agarwal, Coherence decay and its impact on sound radiation by wavepackets, *J. Fluid Mech.* **748**, 399 (2014).
- [78] P. P. C. Brito, P. Morra, A. V. G. Cavalieri, T. B. Araújo, D. S. Henningson, and A. Hanifi, Experimental control of Tollmien-Schlichting waves using pressure sensors and plasma actuators, *Exp. Fluids* **62** (2021).
- [79] F. Lundell, Reactive control of transition induced by free-stream turbulence: An experimental demonstration, *J. Fluid Mech.* **585**, 41 (2007).
- [80] N. Fabianne, Ph.D. thesis, Royal Institute of Technology, 2016.
- [81] K. B. Ariyur and M. Krstić, *Real-Time Extremum-Seeking Control* (Wiley-Blackwell, London, 2003).
- [82] K. Kim, C. Kasnakolu, A. Serrani, and M. Samimy, Extremum-seeking control of subsonic cavity flow, *AIAA J.* **47**, 195 (2009).
- [83] R. Maury, M. Koenig, L. Cattafesta, P. Jordan, and J. Delville, Extremum-seeking control of jet noise, *Int. J. Aeroacoustics* **11**, 459 (2012).
- [84] W. Zhi, C. W. Wong, and Y. Zhou, Dual-input/single-output extremum-seeking system for jet control, *AIAA J.* **56**, 1 (2018).

- [85] D. W. Fan, Y. Zhou and B. R. Noack, Fast triple-parameter extremum seeking exemplified control, *Exp. Fluids* **61**, 152 (2020).
- [86] V. F. Kopiev, I. V. Belyaev, M. Y. Zaytsev, V. A. Kopiev, and G. A. Faranosov, Acoustic control of instability waves in a turbulent jet, *Acoust. Phys.* **59**, 16 (2013).
- [87] O. Bychkov, G. A. Faranosov, V. F. Kopiev, V. A. Kopiev, I. V. Belyaev, I. Moralev, and P. Kazansky, Plasma-based active closed-loop control of instability waves in unexcited jet. Part 1. Free jet, in *Proceedings of the 25th AIAA/CEAS Aeroacoustics Conference, Delft, The Netherlands* (AIAA, Reston, VA, 2019).
- [88] M. Wei and J. Freund, A noise-controlled free shear flow, *J. Fluid Mech.* **546**, 123 (2006).
- [89] J. Kim, D. J. Bodony, and J. B. Freund, Adjoint-based control of loud events in a turbulent jet, *J. Fluid Mech.* **741**, 28 (2014).
- [90] O. Kaplan, P. Jordan, A. V. G. Cavalieri, and G. A. Brès, Nozzle dynamics and wavepackets in turbulent jets, *J. Fluid Mech.* **923**, A22 (2021).
- [91] P. H. Alfredsson and R. Örlü, The diagnostic plot- a litmus of wall-bounded turbulence data, *Eur. J. Fluid Mech. B/Fluids* **29**, 403 (2010).
- [92] J. C. Laurence, Intensity, scale and spectra of turbulence in mixing regions of free subsonic jet, NASA Technical Report No. 19930092288, April 24, 1956; (<https://digital.library.unt.edu/ark:/67531/metadc60688/m1/24/>).
- [93] P. O. A. L. Davies, M. J. Fisher, and M. J. Barrat, The characteristics of turbulence in the mixing region of a round jet, *J. Fluid Mech.* **15**, 337 (1963).
- [94] P. Bradshaw, D. H. Ferris, and R. F. Johnson, Turbulence in the noise-producing region of a circular jet, *J. Fluid Mech.* **19**, 591 (1964).
- [95] J. C. Lau, Laser velocimeter correlation measurements in subsonic and supersonic jets, *J. Sound Vib.* **70**, 85 (1980).
- [96] P. J. Morris and K. B. M. Q. Zaman, Velocity measurements in jets with application to noise source modelling, *J. Sound Vib.* **329**, 394 (2010).
- [97] J. Bridges and M. P. Wernet, Establishing consensus turbulence statistics for hot subsonic jets, in *Proceedings of the 16th AIAA/CEAS Aeroacoustics Conference, Stockholm, Sweden* (AIAA, Reston, VA, 2010).
- [98] R. Örlü and P. H. Alfredsson, On spatial resolution issues related to time-averaged quantities using hot wire anemometry, *Exp. Fluids* **49**, 101 (2010).
- [99] P. Schlatter and R. Örlü, Assessment of direct numerical simulation data of turbulent boundary layers, *J. Fluid Mech.* **659**, 116 (2010).
- [100] B. A. Belson, O. Semeraro, C. W. Rowley, and D. S. Henningson, Feedback control of instabilities in the two-dimensional blasius boundary layer: The role of sensors and actuators, *Phys. Fluids* **25**, 054106 (2013).
- [101] S. Devasia, Should model-based inverse inputs be used as feedforward under plant uncertainty?, *IEEE Trans. Autom. Control* **47**, 1865 (2002).
- [102] G. Tissot, M. Zhang, F. C. Lajús, Jr., A. V. G. Cavalieri, and P. Jordan, Sensitivity of wavepackets in jets to nonlinear effects: The role of the critical layer, *J. Fluid Mech.* **811**, 95 (2017).
- [103] A. V. G. Cavalieri, D. Rodríguez, P. Jordan, T. Colonius, and Y. Gervais, Wavepackets in the velocity field of turbulent jets, *J. Fluid Mech.* **730**, 559 (2013).
- [104] D. Rodríguez, A. V. G. Cavalieri, T. Colonius, and P. Jordan, A study of wavepacket models for subsonic turbulent jets using local eigenmode decomposition of piv data, *Eur. J. Mech. B/Fluids* **49**, 308 (2015).